Journal of Colloid and Interface Science 439 (2015) 62–68

Contents lists available at ScienceDirect

Journal of Colloid and Interface Science

www.elsevier.com/locate/jcis

Enhanced visible-light photocatalytic performance of electrospun carbon-doped TiO_2/halloysite nanotube hybrid nanofibers

Ling Jiang, Yunpeng Huang, Tianxi Liu *

State Key Laboratory of Molecular Engineering of Polymers, Department of Macromolecular Science, Fudan University, Shanghai 200433, PR China

ARTICLE INFO

Article history:
Received 7 September 2014
Accepted 18 October 2014
Available online 24 October 2014

Keywords:
Halloysite
Electrospun TiO_2 nanofibers
Visible-light photocatalyst

ABSTRACT

In this work, the effects of halloysite nanotubes (HNTs) on the visible-light photocatalytic ability of electrospun carbon doped TiO_2/HNT (C—TH) nanofibers have been explored. Structural and morphological investigations demonstrate that incorporation of HNTs into anatase C—TH hybrid nanofibers was easily achieved by using sol–gel processing combined with electrospinning approach, thus HNTs could be uniformly embedded in the electrospun nanofibers. The visible-light photocatalytic efficiency of C—TH hybrid on the degradation of methyl blue (MB) was greatly enhanced with the combination of moderate amount of HNTs (8%), which was 23 times higher than that of commercial anatase TiO_2. Mechanism of the enhancing effect of HNTs has been explored by analyzing the dual-effect of adsorption and photocatalysis in various amounts of HNTs incorporated C—TiO_2 nanofibers. With nanotubular structure and considerable adsorption ability, incorporated HNTs functioned as porogen agent in C—TH nanofibers. This simple incorporation approach increases the specific surface areas of nanofibers, which improves the mass transport of reactant into the nanofibers and the adsorption of visible-light by scattering, meanwhile may suppress the charge recombination and enhance photoinduced charge separation, thus efficiently enhancing visible-light photocatalytic performance of the C—TH hybrid nanofibers.

1. Introduction

Currently, it is highly desirable to develop advanced materials being capable of exploiting clean and renewable solar energy for solving the environmental pollution problems, meanwhile saving energy resources in our planet earth [1–3]. Titanium dioxide (TiO_2) is one of the most promising semiconductor photocatalyst for the chemical utilization of solar energy, which has found world-wide applications in many fields including water/air pollution abatement [4–6]. As is known to all, the photocatalytic property of TiO_2 is derived from the interaction between electron–hole pair (e^-h^+) and molecules close to the photo-excited active centers in catalyst surface. However, the exciton of e^-h^+ pair in pure TiO_2 could only be achieved by ultraviolet (UV) light ($\lambda < 420$ nm) irradiation because of the high band gap energy of TiO_2. Thus, high visible-light (Vis) photocatalytic efficiency of TiO_2 based material mainly relies on a relatively narrower band gap (<3.2 eV for anatase, and <3.0 eV for rutile). In addition, for a fast diffusion of pollutant and an effective utilization of visible-light, materials with high specific surface area are also favorable [7–10].

There are many reports about the composites of TiO_2 and carbonaceous materials for Vis-photocatalysts, which have significantly improved the photocatalytic performance of TiO_2 [11–13]. With impurity states nearing the valence band edge and inhibiting recombination of e^-h^+ pair, doping of carbon atoms or carbonate species could narrow the band gap of TiO_2 and shift the absorption edge to the visible light region [12,14]. Hybridizing TiO_2 with conjugated structural materials including graphene and carbon nanotubes could lower the band gap and act as a visible-light sensitizer during an interfacial charge transfer process [15,16]. Except for the carbon sensitization, other factors such as phase type, thickness of coating-layer [17], morphologies [18] and oxygen vacancy concentration [19] also play important roles in the photocatalytic degradation process. It has been reported that the diffusion path of dye molecule could be increased by loaded carbon via its dye adsorption ability. However, the carbon coating layer decreases the light intensity irradiated on TiO_2 thus degrades the catalytic activity [20]. Hollow microsphere structural carbon modified TiO_2 (CTHS-500) with high surface area and carbon doping amount exhibits a superior visible-light photocatalytic activity for the degradation of toluene than that of CTHS-400 and CTHS-600, which are annealed at different temperatures [21]. Hence, a well-designed and synergistic architecture of TiO_2 based hybrids is important for the advanced photocatalytic performance.

* Corresponding author. Fax: +86 21 65640293.
E-mail address: txliu@fudan.edu.cn (T. Liu).

http://dx.doi.org/10.1016/j.jcis.2014.10.026
0021-9797/

Electrospinning, a simple and versatile technique for the fabrication of one-dimensional (1D) structural fibers, has recently been reported to be advantageous in the separation of e^-h^+ pairs by the vectorial transport of photogenerated charge carriers through the grain boundaries of TiO_2 nanofibers [22]. Furthermore, electrospun TiO_2 nanofibers gain the benefit of recyclability and are free of secondary pollution during the practical applications compared with TiO_2 nanopower. Halloysite ($Al_2Si_2O_5(OH)_4{\cdot}2H_2O$) nanotubes (HNTs) is a type of natural clay with nanotubular structure formed by rolling layers of tetrahedral sheets of silica as outer surface and octahedral sheets of alumina as lumen surface. Growing attention has been attracted on HNTs during recent years due to their excellent adsorption capacity, mechanical property, biocompatibility, unique surface chemical state and cost-effectiveness [23–26]. Several reports have demonstrated that a thin coating of Al_2O_3 or SiO_2 on nanocrystalline TiO_2 films could function as physical barrier for both electron injection and charge recombination reactions in dye sensitized solar cells [27,28]. These work inspired us that halloysites with similar chemical composition would be promising candidates to improve the photocatalytic performance of TiO_2. Besides, many reports have investigated the effects of halloysites in electrospun polymer nanofibers as drug-delivery vehicle for encapsulation and release of drugs [29,30], which demonstrated a good prospect and feasibility of the combination of HNTs and electrospinning.

Herein, we report the fabrication of carbon doped TiO_2/HNT (C—TH) hybrid nanofibers by one-pot electrospinning. The performance of halloysites incorporated composites on the photocatalytic degradation of methyl blue (MB) under visible-light is studied. The enhancing mechanism of HNTs on the catalytic performance and the factors influencing the photocatalytic activity of the C—TH hybrids are discussed.

2. Experimental section

2.1. Materials

Halloysite nanotubes were obtained from Zhengzhou Jinyangguang China Clays Co., Ltd. (China). Poly(vinyl pyrrolidone) (PVP, Mw = 1,300,000) and titanium butoxide (TBT) were purchased from Aladdin Chemical Reagent Co. Ltd. Ethanol and acetic acid were supplied by Sinopharm Chemical Reagent Co., Ltd. All of the reagents were used as received without further purification. Commercial TiO_2 (Sinopharm Chemical Reagent) was used for the blank experiments.

2.2. Preparation of C—TH nanofibers

TBT was used as titanium precursor and PVP functioned as template and carbon source. Typically, 0.64 g TBT, 0.32 g PVP and 50 mg HNTs (mass ratio of TBT:HNTs = 100:8) were dispersed in a mixed solution of ethanol and acetic acid (weight ratio = 3:1), followed by magnetic stirring at ambient temperature for half an hour. Subsequently, the as-formed homogeneous precursor solution was transferred into a plastic syringe for electrospinning at a fixed electrical potential of 10 kV. The electrospinning solution was fed at a speed of 15 mL h^{-1} with a distance of 12 cm between the needle tip and the collector, forming a fiber membrane on a collector of aluminum foil. The electrospun nanofiber membrane were dried overnight at 60 °C to remove residual solvent, then calcined at 500 °C in a crucible covered with a cap under air atmosphere for 2.5 h to obtain C—TiO_2/8% HNT (C—TH-8) hybrid nanofibers (as shown in Scheme 1). By controlling the amount of HNTs, C—TiO_2/HNT hybrid nanofibers with 0%, 4% and 12% HNTs were obtained accordingly, which were abbreviated as C—T, C—TH-4, and C—TH-12, respectively.

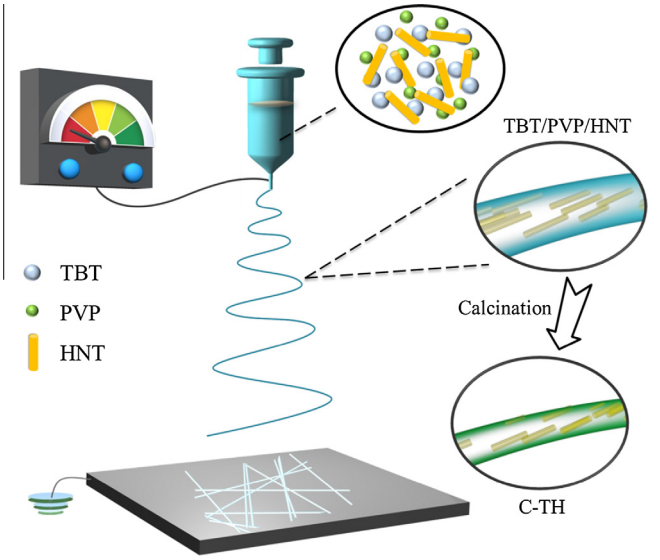

Scheme 1. Schematic illustration of the synthesis of C—TH hybrid nanofibers.

2.3. Characterization

X-ray diffraction (XRD) measurements were conducted on a PANalytical X'Pro X-ray diffractometer (from Netherlands) with Cu Kα radiation (λ = 0.1542 nm) under a voltage of 40 kV and a current of 40 mA. The morphologies of the samples were investigated using a transmission electron microscope (TEM, Tecnai G2 20 TWIN, China) under an accelerating voltage of 200 kV and a field-emission scanning electron microscope (SEM, Ultra 55, Germany) at an acceleration voltage of 20 kV, where TEM samples were prepared by dropping the sample dispersion on the copper grids and dried in air. X-ray photoelectron spectroscopy (XPS) analyses were performed with a VG ESCALAB 220I-XL device (from America) to investigate the surface properties of the samples. All XPS spectra were corrected using C 1s line at 284.6 eV. Curve fitting and background subtraction were accomplished using XPS PEAK 41 software. All electrochemical measurements were performed using a CHI 660D electrochemical workstation (Shanghai Chenhua Instrument Co., China). Methylene blue concentrations were calibrated and determined by UV–vis spectrophotometer (Perkin–Elmer, Lambda 35, America) at a wavelength of 664 nm.

2.4. Evaluation of adsorption and photocatalytic activity

The photocatalytic degradation of MB was performed in a stirred quartz reactor filled with 50 mL MB aqueous solution (20 mg/L) and 10 mg of catalyst. The reactor was equipped with 50WUV lamps with short-wavelength components ($\lambda < 420$ nm) of the light that has been cut off by a glass optical filter. All of the photocatalytic experiments were carried out after the adsorption of MB in the dark for 60 min under stirring. Afterwards, the reactor was exposed to the visible-light irradiation under ambient conditions and rigorous stirring. At certain time intervals, 3 mL of sample solution was taken out during the experiments and centrifuged to remove the catalyst completely, then MB concentration was determined by UV–vis spectrophotometer. For the evaluation of adsorption ability, MB adsorption experiments were carried out in the dark with the same procedure as the photocatalytic experiments described above. The removal percentage by adsorption or

photocatalytic degradation is reported as $(1\text{-}C/C_0) * 100\%$ with time, where C is the concentration of MB at each time interval, and C_0 is the initial concentration. For comparison, a commercial anatase TiO_2 photocatalyst supplied by Sinopharm Chemical Reagent and the mixture of as-prepared C—TiO_2 (C—T) nanofibers with 8 wt% HNTs were tested for their absorptivity and photocatalytic performance using the same procedure and conditions described above.

3. Results and discussion

3.1. Structure and morphology of C—TH hybrid nanofibers

The influence of HNTs on the morphologies of co-electrospun TBT/PVP/HNT hybrid nanofibers and the calcined C—TH hybrids were observed by SEM and TEM, as shown in Figs. 1 and 2, respectively. For different amounts of HNT loading, their fiber diameters were carefully controlled by tuning the electrospinning parameters, e.g., voltage, feeding rate and collecting distance. As shown in Fig. 1, the average diameters of TBT/PVP/HNT nanofibers with 0%, 4%, 8% and 12% HNTs were all about 350 nm to eliminate the influence of fiber diameter on photocatalytic or adsorption. It can be observed that surface roughness of TBT/PVP/HNT hybrid nanofibers is getting more obvious when increasing the amount of HNTs, probably due to the rigid nanostructure and weak conductivity of HNTs. As shown in typical TEM image (Fig. 2b), HNTs were uniformly distributed along the nanofibers and few aggregations can be seen in the TBT/PVP/HNT-8 nanofibers. After calcination, TBT precursor was transformed into TiO_2 meanwhile the spinnable component of PVP was carbonized and doped onto TiO_2. The as-prepared C—T, C—TH-4 and C—TH-8 hybrid nanofibers retained their uniform morphology, with the diameter of about 180, 210 and 240 nm (Fig. 1c, f and i), respectively. Also, as indicated by the arrows, HNTs were uniformly distributed in C—TH-8 hybrid nanofibers (Fig. 2c), demonstrating that combination of one-dimensional (1D) electrospun nanofibers and one-dimensional (1D) hollow nanotubes has been achieved to form C—TH hybrid nanofibers. Mesoporous structure of TiO_2 in C—TH hybrid nanofibers can be seen from the high magnification TEM image (Fig. 2d), composing a multi-aperture C—TH hybrid nanofiber by combining the nanotubular structure of HNTs. Interestingly, the diameters of the C—TH-12 hybrid nanofibers varied from 30 nm to 260 nm, and some spindle-shaped aggregates of HNTs protruded out of the hybrid nanofibers (Fig. 1l), probably ascribing to the high concentration of HNTs that results in an aggregation tendency in the sol–gel process. All of these confirm that a moderate amount of HNTs is of great importance for getting the uniform distribution of HNTs in the C—TH hybrids.

The crystal structure of C—TH hybrid nanofibers was characterized by XRD. As shown in Fig. 3, the XRD patterns of C-TH hybrid nanofibers with 0%, 4%, 8% and 12% HNTs all exhibit strong diffraction peaks at 2θ values of 25.6° (101), 38.4° (004), 48.3° (200), 55.2° (105), and 63.3° (204), which can be assigned to anatase structure of TiO_2 (PDF No. 84-186). With increasing the amount of HNTs, intensity of diffraction peaks assigned to HNTs in C—TH hybrid nanofibers increases, in accordance with SEM observation that higher HNT loading may lead to the exposure of HNTs on the fiber surface of the C—TH hybrids. All of these demonstrate that HNTs have been successfully embedded into the electrospun hybrid nanofibers.

Chemical states of incorporated dopants in the as-prepared C—TH hybrid catalysts were determined by XPS analysis. Results of survey, Ti 2p, C 1s and O 1s spectra were shown in Fig. 4. Three peaks at 284.6, 285.4 and 288.6 eV were observed in C 1s (Fig. 4c). The peak at 284.6 eV is usually assigned to sp^2 hybridized C atoms [31,32], and there are varied carbon oxidation states in carbon doped titanium caused by different preparation methods. However, the peak at 281 eV corresponding to Ti—C bond was not observed, indicating that oxygen atom does not be substituted by carbon in the lattice of anatase. Peaks at 285.4 and 288.6 eV can

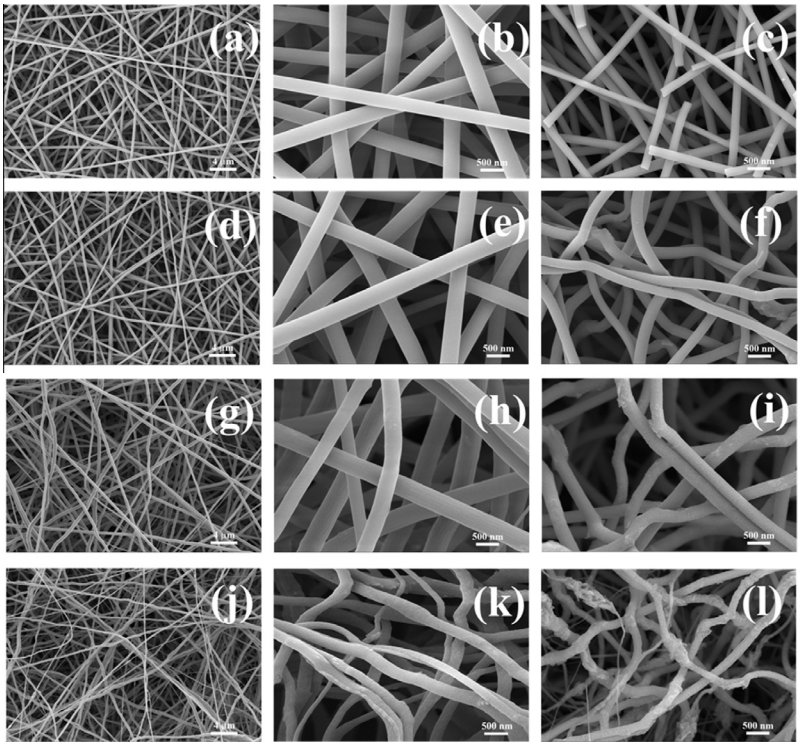

Fig. 1. Typical SEM micrographs of electrospun (a, b) TBT/PVP and TBT/PVP/HNT hybrid with (d, e) 4%, (g, h) 8% and (g, k) 12% HNTs (relative to TBT) doped at low and high magnifications, respectively. (c) C—T, (f) C—TH-4, (i) C—TH-8 and (l) C—TH-12 hybrids were obtained from related electrospun nanofibers after calcining, respectively.

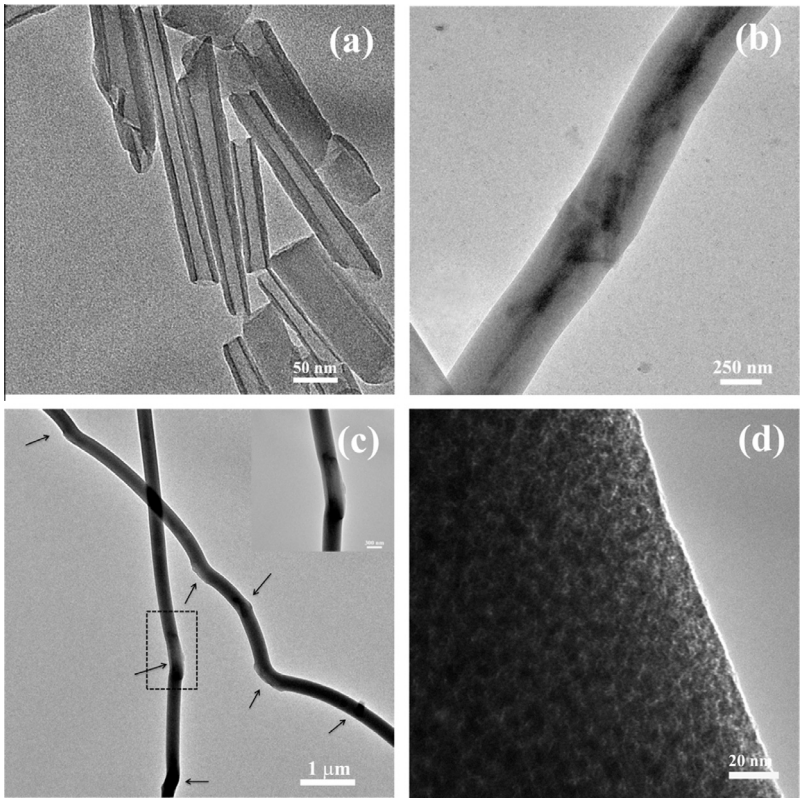

Fig. 2. Transmission electron micrographs of (a) HNTs, (b) electrospun TBT/PVP/HNT-8 and C—TH-8 hybrids at (c) low and (d) high magnifications. The inset image in (c) is TEM of the dashed box at high magnification.

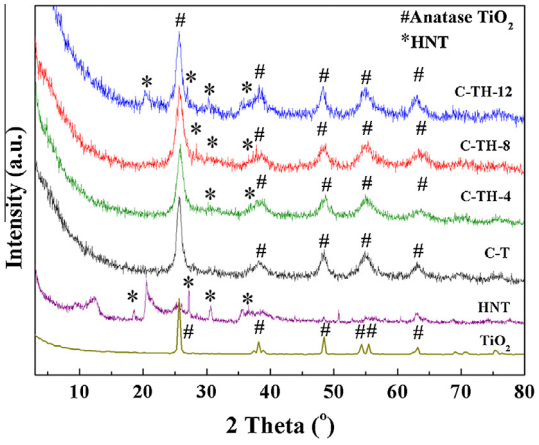

Fig. 3. XRD patterns of commercial TiO_2, HNT, C—T, C—TH-4, C—TH-8 and C—TH-12 hybrids. The diffraction peaks of HNT and anatase TiO_2 are labeled as ∗ and #, respectively.

be ascribed to C—O and C═O bonds in carbonate species, revealing that carbon may substitute for some of the lattice titanium atoms to form a Ti—O—C structure. These carbonate species might be incorporated into the interstitial position of TiO_2 lattice and play a role of inhibiting the electron–hole recombination as reported elsewhere [12,33]. The concentration of carbonate species was estimated to be 7.5 atom% from the peak areas of C 1s associated with carbonate species, Ti $2p_{3/2}$ and O 1s. It has been reported that an obvious long-tail adsorption in visible region was assigned to the carbonate species in C-doped TiO_2 [12,34]. Thus it is more reasonable for the enhanced visible-light activity of the as-prepared C—TH hybrids. As shown in Fig. 4b, XPS signals of Ti 2p were observed at binding energies at 458.4 (Ti $2p_{3/2}$) and 464.3 eV (Ti $2p_{1/2}$), which is consistent with the formation of crystalline TiO_2. The peaks at binding energies of 532.5, 531.3 and 529.7 eV in O 1s can be assigned to O—H, C═O and O—Ti bond, respectively (Fig. 4d), drawing the same conclusion of the successful formation of carbonate species in TiO_2 lattice. Oxygen vacancy concentration can be evaluated from the XPS results. By calculating ratios between the O—Ti percentages from the O 1s spectra and the Ti atom percentage from the XPS survey spectra, we can estimate the x number of O atoms bonded with Ti^{4+} in TiO_x. It is found that x value of the as-prepared C—TiO_x/HNT-8 hybrid is about 1.84, which corresponds to oxygen vacancy concentration at 8% and thus results in a higher catalytic activity than defect-free surfaces [35].

3.2. Photocatalytic activity

The effect of HNTs in photocatalytic activities of the as-prepared C-TH hybrid nanofibers was studied by the photocatalytic degradation of MB under visible-light irradiation. Fig. 5 shows the UV–vis diffuse reflectance spectra of MB solution before and after visible-light ($\lambda > 420$ nm) irradiation for different exposure time in the presence of C—TH hybrids with 0%, 4%, 8% and 12% amounts of HNTs. The C—T nanofibers show a poor photocatalytic activity under visible-light (Fig. 5a), which is assigned to the limited doped carbon and oxygen vacancies. However, obvious decrease on the absorbance intensity has been shown in different C—TH hybrids at the same exposure time compared to C—T nanofibers (Fig. 5b–d), demonstrating enhancing effect of HNTs in the visible-light photocatalytic performance. By comparing the characteristic absorption bands of MB solution at 664 nm (Fig. 5), the visible-light photocatalytic performance was improved with an ascending order from C—TH-4, C—TH—12 to C—TH-8 nanofibers, where C—TH-8 hybrid exhibits the best performance on MB degradation by 73% in 80 min.

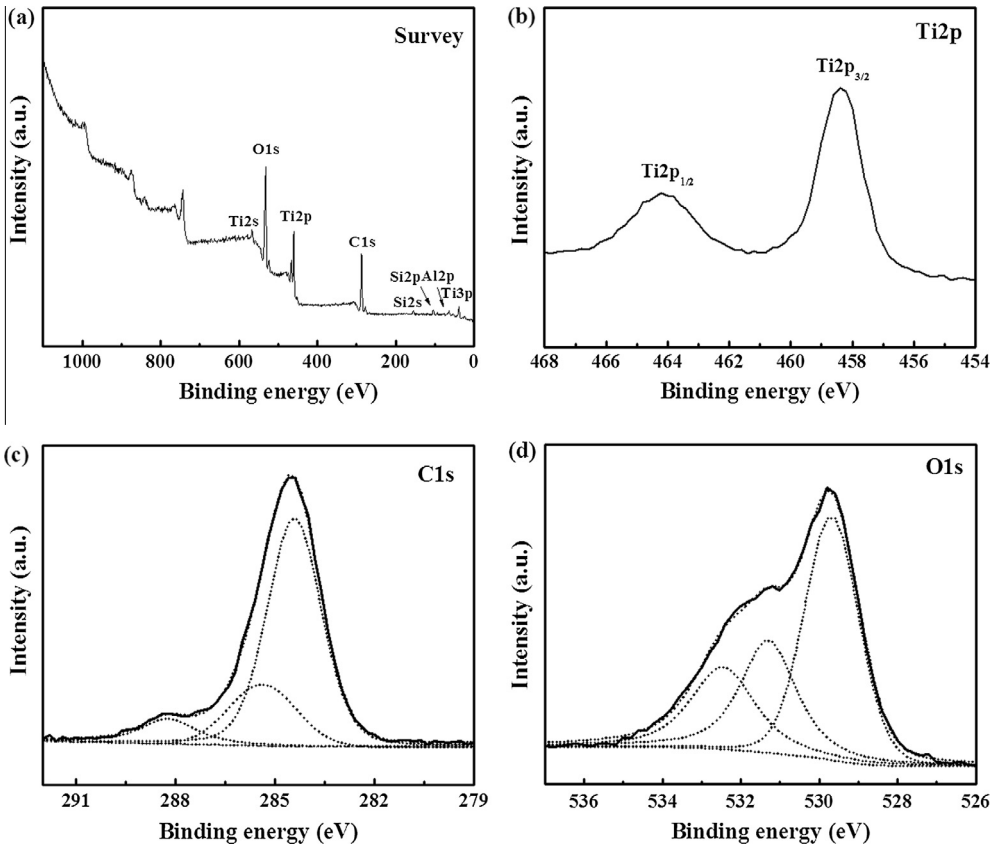

Fig. 4. XPS spectra of (a) survey, (b) Ti2p, (c) C 1s and (d) O 1s of the C—TH-8 hybrid nanofibers.

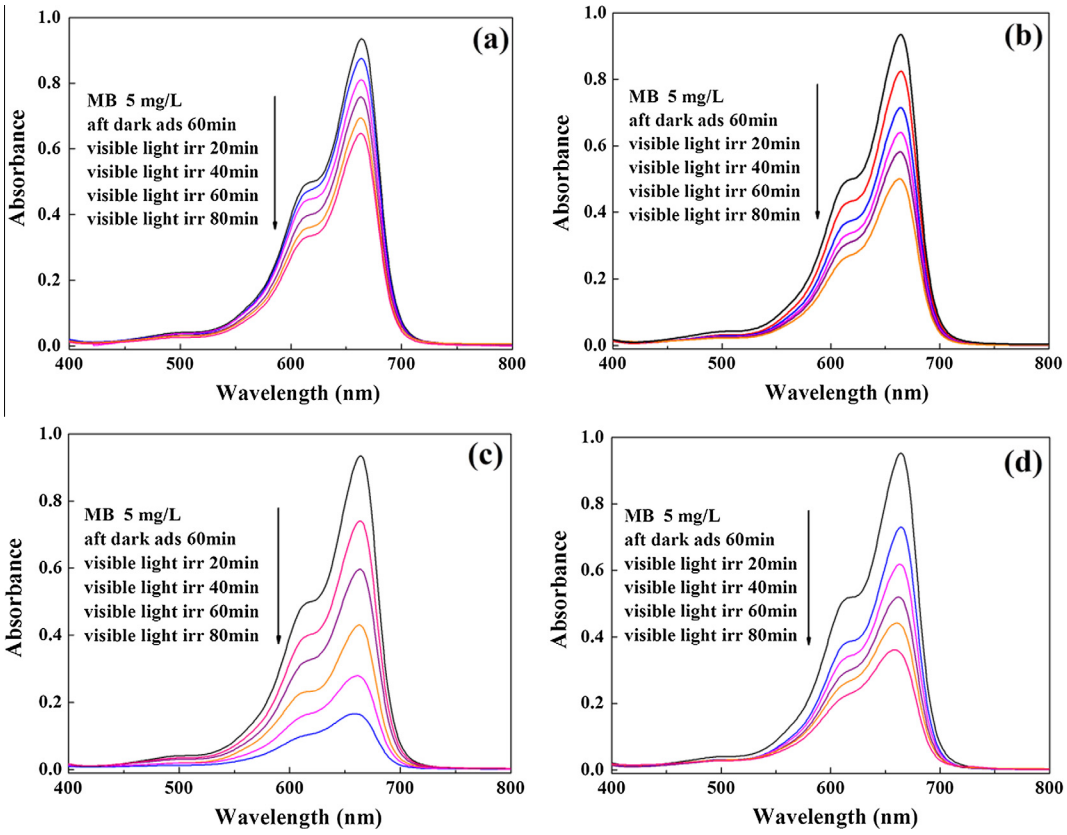

Fig. 5. Photocatalytic degradation of methylene blue under visible-light ($\lambda > 420$ nm) in the presence of C—T (a), C—TH-4 (b), C—TH-8 (c) and C—TH-12(d) hybrid nanofibers in time intervals of 0, 20, 40, 60 and 80 min after 60 min storage in dark for excluding the interference of adsorption.

In order to explore the enhancing mechanism of HNTs on the photocatalytic activity, commercial available anatase TiO_2 powder and the mixture of C—T nanofibers and 8% halloysite powder (C—T/H-8) were used for MB degradation for comparison with the C—TH hybrid nanofibers. Adsorption in dark was also carried out to investigate the effect of adsorption on the photocatalytic activity (Fig. 6a). 1-C/C_0 was used in adsorption and photocatalysis to characterize the relative degradation capacity. As can be seen from Fig. 6a, adsorption ability was improved by incorporating HNTs into electrospun C—T nanofibers, and the equilibrium adsorption capacity was in an ascending order of TiO_2, C—T, C—TH-4, C—TH-8, C—T/H-8 and C—TH-12. Clearly, increasing the amount of incorporated HNTs has a positive effect on the adsorption ability of C—TH hybrid nanofibers. Interestingly, the as-prepared C—TH-8 nanofibers exhibited comparable adsorption ability with the mixture of C—T and 8% halloysites. Thus it can be concluded that there is no negative effect of incorporated HNTs on the adsorption ability of MB, probably due to the mesoporous structure of the C-TH hybrid nanofibers (Fig. 2d).

Fig. 6b shows the photocatalytic degradation percentage of MB versus time under visible-light for all samples. It can be seen that the degradation performance of commercial TiO_2 is negligible. Whereas, notable improvements of HNTs incorporated C—TH hybrids on the degradation of MB have been achieved. Quantitative evaluation of the photocatalytic activities was performed by the first order reaction rate constants (k_1) as listed in Table 1. The increasing order of the rate constants in the samples is: TiO_2 < C—T < C—T/H-8 < C—TH-4 < C—TH-12 < C—TH-8. The rate constant exhibits a maximum of 0.018 min^{-1} for C—TH-8 hybrid nanofibers,

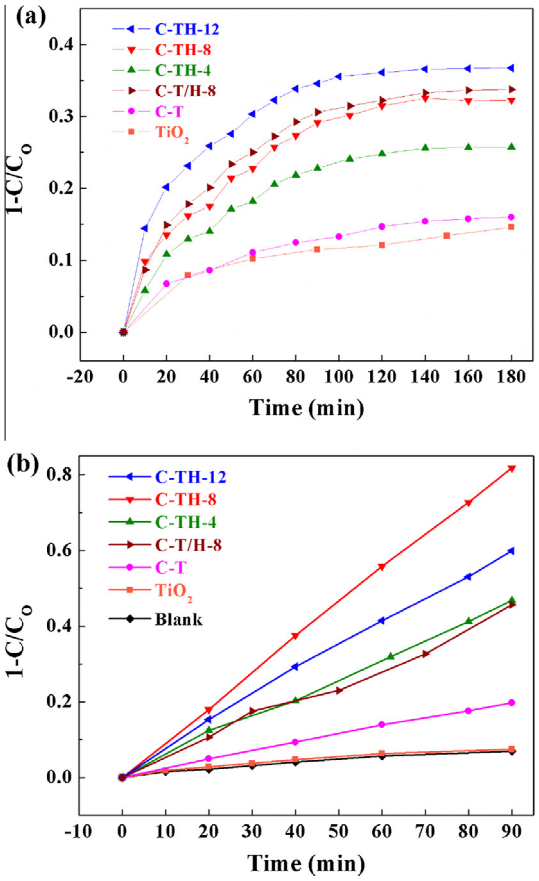

Fig. 6. Adsorption rate of MB in dark (a) and changes in the relative concentrations of MB under visible-light irradiation after 60 min storage in dark (b) on commercial TiO_2, C—T, C—TH hybrids and the mixture of C—T and 8% HNT (C—T/H-8), respectively. MB concentration: 50 mg L^{-1}, catalyst dosage: 0.4 mg mL^{-1}, temperature: 298 K.

Table 1
Kinetic parameters for photocatalytic activities of the C—TH hybrid nanofibers by first-order-reaction.

	TiO_2	C—T	C—TH-4	C—TH-8	C—TH-12	C—T/H-8
$k_1/10^{-3}$ min^{-1}	0.8	2.4	7.0	18.4	10.0	6.4
R^2	0.9733	0.9994	0.9909	0.9856	0.9923	0.9469

which is 23 and 7.6 times higher than that of commercial TiO_2 and the as-prepared C—T nanofibers under the same condition, respectively. Besides, the rate constants of C—TH-4 and C—TH-12 hybrids are also much higher than that of C—T nanofibers without incorporation of HNTs, which are 2.9 and 4.1 times higher, respectively. Thus, by increasing the amount of incorporated HNTs in the electrospun C—TH nanofibers in an appropriate range, visible-light photocatalytic activity could be significantly improved.

It is well accepted that the photocatalytic effect in solid-state catalysis was caused by the electro-hole pair (e^-h^+) created from photon adsorption interacted with molecules close to the catalyst surface [2]. Therefore, better adsorption ability of the photocatalyst is one of the prerequisites for a better photocatalytic activity, because molecules could more efficiently diffuse to the photo-excited active centers. However, adsorption is not the sufficient condition that conduces to the variation of the photocatalytic performance. The dispersion state of halloysite in the C—TH hybrid nanofibers is proved to be an important factor in this work that affects the photocatalytic performance. As the halloysite nanotubes are uniformly distributed in the hybrid and interwoven with TiO_2, the interfacial diffusion rate of MB to the active centers of TiO_2 could be high. Therefore, the mixture of C—T/H-8 with few interactions between halloysite powders and TiO_2 nanofibers exhibits the poorest photocatalytic performance and the C—TH-8 with even distribution of halloysite shows better photocatalytic ability than that of C—TH-12. Thus, the enhancing effect of photocatalytic activity on the C—TH nanofibers can be ascribed to the hollow nanotubular structure of halloysite with high specific surface areas and considerable adsorption ability that makes the diffusion of reactants into inner nanofibers easier and improves the light adsorption by scattering. Besides, the surface chemical structures of rolling silica tetrahedral layers and alumina octahedral layers with a higher conduction band edge in halloysites may probably modulate interfacial electron transfer dynamics, thus increasing the physical separation of injected electrons and decreasing the charge recombination reactions as reported [27,28]. All of these factors can greatly enhance photoinduced charge separation and transportation in the process of photocatalysis. Except for the enhanced contact areas and the effect of porogen incorporated by HNTs, distribution state of HNTs is another important factor that determines the photocatalytic activity. When the loading amount of HNTs reaches to a relative high value (here, 12%), HNTs tend to aggregate in the nanofibers and the rate constant is lower than that of C—TH-8 hybrid nanofibers with uniformly dispersed halloysite in the nanofibers, demonstrating the negative effect of poor distribution on improving the photocatalytic activity. Furthermore, the reaction rate constant of the mixture of C—T and 8% HNTs is much lower than that of C—TH-8 hybrid nanofibers. Thus a simultaneous effect of HNTs and C—T nanofibers has been achieved for significantly enhancing the visible-light photocatalytic degradation ability in an easy and efficient way.

4. Conclusions

Halloysite nanotubes have been successfully incorporated into electrospun carbon doped anatase TiO_2/HNT hybrid (C—TH) nanofibers via one-pot electrospinning method combining sol–gel

processing. The uniform fibrous structure of electrospun TBT/PVP/HNT hybrid fibers does not significantly change after incorporation of HNTs. The photocatalytic performance of the C—TH hybrids is significantly improved after the incorporation of HNTs into nanofibers. Effects of loading amounts and distribution states of HNTs in the hybrid nanofibers on the photocatalytic activity under visible-light are systemically analyzed. Moreover, C—TH-8 nanofibers exhibit the superior visible-light photocatalytic activity for the degradation of MB, which is 23, 7.6 and 2.9 times higher than that of commercial anatase TiO_2, C—T and the mixture of C—T nanofibers and 8% HNT powder, respectively. Nanotubular HNTs function as active porogen that increases high specific surface areas of the C—TH nanofibers, thus improves the mass transport of reactant into the active centers of nanofibers and the adsorption of visible-light by scattering. Besides, considerable adsorption ability and the uniform distribution of HNTs in C—TH nanofibers make it an easier diffusion of reactants towards the photo-excited active centers in nanofibers. Furthermore, chemical structure of HNTs with higher conduction band edge may decrease the charge recombination and enhance photoinduced charge separation. Thus, incorporating HNTs into C—TH hybrid nanofibers is an efficient and simple way for enhancing the visible-light photocatalytic activity. Therefore, the strategy of incorporating inorganic hollow nanotubes for preparing multi-aperture electrospun hybridized catalyst provides a possible way for remarkable enhancement of the visible-light photocatalytic activity.

Acknowledgment

The authors are grateful for the financial support from the National Natural Science Foundation of China (51125011, 51373037).

References

[1] S.U.M. Khan, M. Al-Shahry, W.B. Ingler, Science 297 (2002) 2243.
[2] J.H. Park, S. Kim, A.J. Bard, Nano Lett. 6 (2006) 24.
[3] A. Pandikumar, R. Ramaraj, J. Renew, Sustain. Energy 5 (2013) 043101.
[4] Y.Z. Li, D.S. Hwang, N.H. Lee, S.J. Kim, Chem. Phys. Lett. 404 (2005) 25.
[5] Z.L. He, W.X. Que, J. Chen, X.T. Yin, Y.C. He, J.B. Ren, ACS Appl. Mater. Interfaces 4 (2012) 6816.
[6] H.G. Yang, C.H. Sun, S.Z. Qiao, J. Zou, G. Liu, S.C. Smith, H.M. Cheng, G.Q. Lu, Nature 453 (2008) 638.
[7] S. In, A. Orlov, R. Berg, F. García, S. Pedrosa-Jimenez, M.S. Tikhov, D.S. Wright, R.M. Lambert, J. Am. Chem. Soc. 129 (2007) 13790.
[8] Y. Cong, J.L. Zhang, F. Chen, M. Anpo, J. Phys. Chem. C 111 (2007) 6976.
[9] J. Yu, Y.L. Yang, R.Q. Fan, L. Li, X.Y. Li, J. Phys. Chem. C 118 (2014) 8795.
[10] D.M. Chen, G.X. Du, Q. Zhu, F.S. Zhou, J. Colloid, Interf. Sci. 409 (2013) 151.
[11] S. Sakthivel, H. Kisch, Angew. Chem. Int. Ed. 42 (2003) 4908.
[12] D.E. Gu, Y. Lu, B.C. Yang, Y.D. Hu, Chem. Commun. (2008) 2453.
[13] P. Zhang, C.L. Shao, Z.Y. Zhang, M.Y. Zhang, J.B. Mu, Z.C. Guo, Y.C. Liu, Nanoscale 3 (2011) 2943.
[14] T. Ohno, T. Tsubota, K. Nishijima, Z. Miyamoto, Chem. Lett. 33 (2004) 750.
[15] Y.H. Zhang, Z.R. Tang, X.Z. Fu, Y.J. Xu, ACS Nano 4 (2010) 7303.
[16] K. Woan, G. Pyrgiotakis, W. Sigmund, Adv. Mater. 21 (2009) 2233.
[17] M. Inagaki, F. Kojin, B. Tryba, M. Toyoda, Carbon 43 (2005) 1652.
[18] D. Sarkar, K.K. Chattopadhyay, ACS Appl. Mater. Interfaces (2014) 10044.
[19] J. Graciani, Y. Ortega, J. Fdez Sanz, Chem. Mater 21 (2009) 1431.
[20] B. Tryba, A.W. Morawski, T. Tsumura, M. Toyoda, M. Inagaki, J. Photochem. Photobiol., A 167 (2004) 127.
[21] H.Q. Wang, Z.B. Wu, Y. Liu, J. Phys. Chem. C 113 (2009) 13317.
[22] S.K. Choi, S. Kim, S.K. Lim, H. Park, J. Phys. Chem. C 114 (2010) 16475.
[23] E. Abdullayev, Y. Lvov, J. Mater. Chem. B 1 (2013) 2894.
[24] E. Abdullayev, V. Abbasov, A. Tursunbayeva, V. Portnov, H. Ibrahimov, G. Mukhtarova, Y. Lvov, ACS Appl. Mater. Interfaces 5 (2013) 4464.
[25] E. Abdullayev, A. Joshi, W. Wei, Y.F. Zhao, Y. Lvov, ACS Nano 6 (2012) 7216.
[26] Y.F. Zhao, E. Abdullayev, A. Vasiliev, Y.R. Lvov, J. Colloid, Interf. Sci. 406 (2013) 121.
[27] E. Palomares, J.N. Clifford, S.A. Haque, T. Lutz, J.R. Durrant, Chem. Commun. (2002) 1464.
[28] E. Palomares, J.N. Clifford, S.A. Haque, T. Lutz, J.R. Durrant, J. Am. Chem. Soc. 125 (2002) 475.
[29] Y.L. Zhao, S.G. Wang, Q.S. Guo, M.W. Shen, X.Y. Shi, J. Appl. Polym. Sci. 127 (2013) 4825.
[30] R.L. Qi, R. Guo, M.W. Shen, X.Y. Cao, L.Q. Zhang, J.J. Xu, J.Y. Yu, X.Y. Shi, J. Mater. Chem. 20 (2010) 10622.
[31] M. Seredych, A.V. Tamashausky, T.J. Bandosz, Adv. Funct. Mater. 20 (2010) 1670.
[32] P.X. Han, Y.H. Yue, Z.H. Liu, W. Xu, L.X. Zhang, H.X. Xu, S.M. Dong, G.L. Cui, Energy Environ. Sci. 4 (2011) 4710.
[33] C. Di Valentin, G. Pacchioni, A. Selloni, Chem. Mater. 17 (2005) 6656.
[34] Z.B. Wu, F. Dong, W.R. Zhao, H.Q. Wang, Y. Liu, B.H. Guan, Nanotechnology 20 (2009) 235701.
[35] M.A. Henderson, W.S. Epling, C.H.F. Peden, C.L. Perkins, J. Phys. Chem. B 107 (2002) 534.